

Profile retrieval of a buried periodic structure using spin echo grazing incidence neutron scattering

Cite as: Appl. Phys. Lett. **116**, 101602 (2020); doi: [10.1063/1.5140616](https://doi.org/10.1063/1.5140616)

Submitted: 30 November 2019 · Accepted: 3 March 2020 ·

Published Online: 12 March 2020



View Online



Export Citation



CrossMark

R. Ashkar,^{1,a)} R. M. Dalgliesh,² R. Pynn,³ A. D. F. Dunbar,⁴ R. A. L. Jones,⁵ and A. J. Parnell^{5,a)}

AFFILIATIONS

¹Department of Physics, Virginia Tech Blacksburg, Blacksburg, Virginia 24060, USA

²ISIS Pulsed Neutron and Muon Source, Science and Technology Facilities Council, Rutherford Appleton Laboratory, Harwell Science and Innovation Campus, Didcot OX11 0QX, United Kingdom

³Physics Department, Indiana University, Bloomington, Indiana 47405, USA

⁴Department of Chemical and Biological Engineering, Sir Robert Hadfield Building, University of Sheffield, Sheffield S1 3JD, United Kingdom

⁵Department of Physics and Astronomy, University of Sheffield, Sheffield S10 2TN, United Kingdom

^{a)}Authors to whom correspondence should be addressed: ashkar@vt.edu and a.j.parnell@sheffield.ac.uk

ABSTRACT

When the neutron scattering technique, Spin Echo Resolved Grazing Incidence Scattering (SERGIS) concept, was originally put forward by Rekveldt [Physica B **1135**, 234–236 (1997)] and Felcher *et al.* [Proc. SPIE **4785**, 164 (2002)], they recognized that the specular scattering and the off-specular scattering could be spatially separated due to the tight neutron beam collimation in the scattering plane, a necessity for any reflectometry experiment. In this Letter, we show that it is possible to make large area measurements of periodic grating structures using SERGIS in a number of interesting scenarios. The SERGIS data can be analyzed using a dynamical theory, which makes it possible to effectively retrieve the lateral profile of a commercial periodic diffraction grating. Interestingly, this is still the case even when that grating is buried beneath a highly deuterated poly(methyl methacrylate-D8) polymer layer. We also clearly demonstrate that the maximum sensitivity to lateral structures is achieved when the specular reflection from the grating is excluded from the data analysis, demonstrating a feature of SERGIS that was proposed over two decades ago.

© 2020 Author(s). All article content, except where otherwise noted, is licensed under a Creative Commons Attribution (CC BY) license (<http://creativecommons.org/licenses/by/4.0/>). <https://doi.org/10.1063/1.5140616>

The long-established technique of specular neutron reflectivity has provided unique information, with an Å-scale resolution, about depth profiles and interfaces in a variety of soft as well as hard matter material systems.^{1–3} In stark contrast to this, the use of neutron reflectivity to resolve lateral structures has been considerably more problematic due to the difficulty in detecting and analyzing off-specular signals that result from such structures.⁴ The most significant problems arise from the combination of low neutron flux and the weakness of the off-specular signal (several orders of magnitude less intense than the specular signal). Even when the off-specular signal is detectable, such as is sometimes the case for periodic structures,^{5–7} finding the appropriate theoretical framework for the analysis and interpretation of the scattering signal is not straightforward. In most instances, the appropriateness and uniqueness of any model used to describe reflectivity data relies on further knowledge about the system under study. In conventional specular reflectivity experiments, another contrast like x-ray reflectivity or

ellipsometry, for example, can provide this information.^{8,9} However, the situation is much more complicated for modeling the off-specular signal, where several approximate scattering theories [Born approximation, the distorted wave Born approximation (DWBA),^{10–14} or phase-object approximation (POA)]¹⁵ have been applied to different systems with varying degrees of success. This applies as well to grazing-incidence techniques other than reflectometry, such as Grazing Incidence Small Angle Neutron Scattering (GISANS). It is worth mentioning that while some GISANS measurements have been made successfully,^{16,17} the technique is, however, limited by neutron beam intensity because tight collimation of the neutron beam is usually needed.

Grazing-incidence scattering techniques are well-suited for the investigation of layered nanopatterned materials; a few studies have used waveguide-enhanced grazing-incidence scattering of x-rays¹⁸ and neutrons¹⁹ to probe buried nanostructures in thin films. The challenge

in these approaches, like most other standard grazing-incidence scattering techniques, is that they simultaneously and indiscriminately measure both specular and non-specular signals in which case the measured intensity is dominated by the more intense specular signal. However, information of lateral structures is mostly embedded in the non-specular signal, which is usually weak and often subtends a wide scattering angle, such that it is only partially captured by the detector. Hence, to get full information about lateral nanostructures, the non-specular signal should ideally be brighter and separated from the specular signal.

Fortunately, one technique that allows for such measurements is Spin-Echo Resolved Grazing Incidence Scattering technique (SERGIS).^{18–21} The advantage of SERGIS over other standard scattering techniques arises from the interferometric properties of this approach in that SERGIS returns real space correlations, providing insight into the length scales possible even without modeling the data. In contrast, conventional scattering techniques return data in reciprocal space, which necessitates a modeling framework to interpret the data obtained.

The SERGIS setup uses an arrangement of trapezoidal magnetic coils to split a polarized neutron beam into two mutually coherent sub-beams of opposite spin states,^{22,23} analogous to Wollaston prisms, used in optical applications for decomposing light into orthogonal polarization states. The phase acquired by each neutron spin state depends on its trajectory through the magnetic prisms, which are designed such that the components before and after the samples are magnetic mirror-images of each other relative to the sample position. To perform these SERGIS measurements, we used the OffSpec neutron reflectometer at the ISIS Pulsed Neutron and Muon Source (Oxfordshire, UK).^{24–28} This instrument uses neutron wavelengths of 2–12 Å. Measurements were performed for spin up (I^+) and spin down (I^-), by flipping the spin of the scattered beam immediately before the analyzer. Besides accessing the intensity of the scattered beam in both spin states, this also enables the measurement of the polarization, $P = \frac{I^+ - I^-}{I^+ + I^-}$, on the same sample in the same scattering geometry as well as comparison of the profile sensitivity of the signal in both states. The OffSpec instrument uses shaped coils and RF flippers to achieve encoding of the neutron beam, and further technical details can be found in the study by Ashkar *et al.*²⁹ For the case in which a sample only reflects specularly, the symmetry of the magnetic fields ensures that there is no overall phase difference between the spin states. In this case, the initial polarization state of the neutrons is fully recovered after the apparatus, a condition known as a spin echo. However, should lateral structures in the sample cause scattering in the y -direction (see Fig. 1), then the two spin states will experience

different trajectories and interfere to yield a reduced neutron polarization. The measurements are usually interpreted in terms of the normalized polarization, $P_{\text{normalized}}$, defined as the polarization, P , measured from the sample and divided by the polarization, P_0 , measured from a non-structured specularly reflecting silicon/quartz wafer, such that $P_{\text{normalized}} = P/P_0$ and hence removing instrumental contributions to the measurement, with an unstructured sample having a $P_{\text{normalized}}$ value equal to 1.

The apparatus sketched in Fig. 1 allows for relaxed collimation of the neutron beam perpendicular to the specular reflection; i.e., in the y direction, without a concomitant loss of resolution or reduction in scattered neutron intensity. Since the technique simultaneously measures specular and off-specular scattering events, the measured polarization signal is the sum of these two contributions. The overall signal is usually dominated by the specular beam, reducing the accuracy with which the polarization of the off-specular scattering signal can be measured. However, when SERGIS was originally proposed by Rekveldt²⁰ and Felcher *et al.*,²¹ they recognized that the specular beam and off-specular scattering could be separated because of the tight neutron beam collimation in the scattering plane (i.e., the xz plane of Fig. 1) required for any reflectometry experiment. This means that the specular scattering covers only a small area on the neutron detector, whereas off-specular scattering covers a larger area, and so the two can be separated.

For periodic samples, such as the grating studied here, the normalized SERGIS polarization signal can be expressed as

$$\frac{P}{P_0} = \sum_m \tilde{p}_m \cos(mg\zeta), \quad (1)$$

where m is an integer labeling the order of the Bragg reflection from the grating, \tilde{p}_m is the scattering probability of the scattered beam of order m , $g = 2\pi/d$ is the smallest reciprocal lattice vector (d being grating period), and ζ is the spin-echo length given by $\zeta = c\lambda^2$,³⁰ in which c is a constant determined by instrument geometry (herein $c = 3010/\text{nm}$) and λ is the neutron wavelength. For a detailed figure of the scattering geometry, the reader is referred to Fig. 2 in the study by Ashkar *et al.*²⁹

In this Letter, we demonstrate that the SERGIS technique,^{21–23} combined with a dynamical theory formalism for calculating Eq. (1), provides excellent sensitivity to both the in-depth composition and lateral morphologies of buried periodic nanostructures, especially when specular scattering and off-specular scattering are analyzed separately.

The difference between the two types of measurements is evident in the polarization and conventional intensity detector maps shown in Fig. 2. It is clear that the unpolarized datasets (a–c) do not show any observable intensity modulations (within the resolution) pertaining to

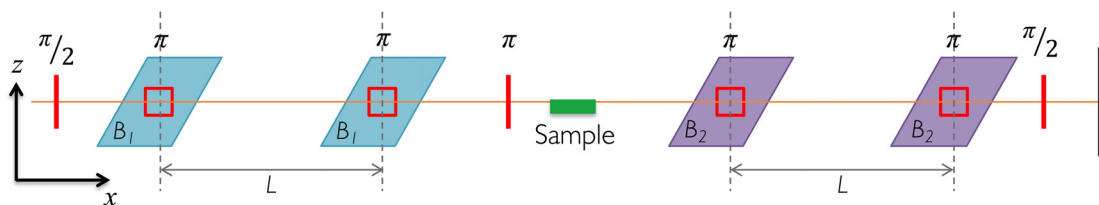


FIG. 1. A schematic of the trapezoidal magnetic fields used for the Larmor encoding system. The neutron beam goes from left to right. Prior to the sample, the neutrons are split into two beams with opposite polarizations. The separation is in the y direction of the two spin states with spin echo length ζ . The scattering geometry is such that the xz plane is the neutron scattering plane for specular scattering from the sample, and scattering in the y direction corresponds to GISANS.

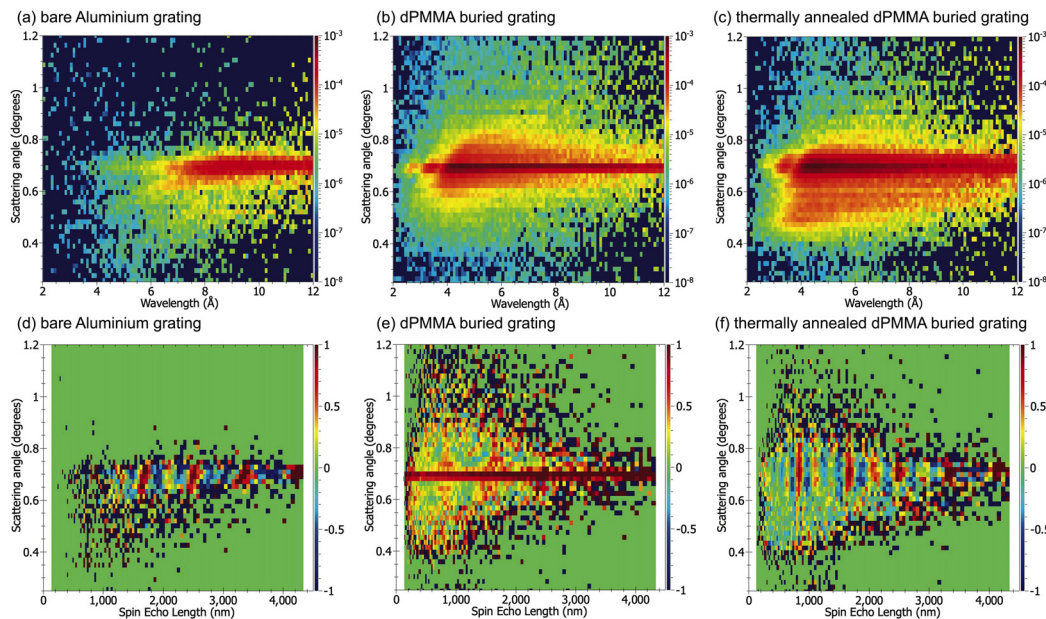


FIG. 2. Scattering maps for the unpolarized scattering ($I^+ + I^-$) from the samples (a)–(c) and corresponding SERGIS signal (d)–(f) measured as $\frac{I^+ - I^-}{(I^+ + I^-)}$. The three samples are uncoated aluminum grating (a) and (d), dPMMA buried grating (b) and (e), and thermally annealed dPMMA grating (c) and (f).

the periodic structure of the grating, even when it is most likely to see them, i.e., with the bare grating, because the unmodulated specular scattering dominates. This is partly due to the scattering geometry that yields Bragg beams that are too close to the specular ridge and cannot be resolved with the pixel size of the detector. In comparison, the SERGIS polarized 2D detector maps, Figs. 2(d)–2(f), show strong regular repeating features that can be seen for all three cases. The most remarkable observation, however, is that the modulated polarization features, although quite damped, are still detectable in the signal from the unannealed dPMMA coated grating away from the specular ridge.

This modulation in the polarization signal around the specular ridge is depicted in the integrated SERGIS polarization shown in Fig. 3. The integration was performed in three ways: over the entire detector and over three detector pixels subtending an angular range of $\approx 0.25^\circ$ above and also below the specular ridge.

The analysis of the SERGIS data was performed using a dynamical theory (DT) code developed in detail in the study by Ashkar *et al.*²⁹ and also in Refs. 31 and 32. Unlike approximate scattering theories, such as DWBA and POA, the dynamical theory model used in this work is an exact theory for the analysis and interpretation of off-specular Bragg scattering from a perfectly periodic material. The model has been tested and verified on a number of samples and has been shown to sensitively reproduce fine features of the SERGIS signals in various scattering geometries. Additionally, the model has a built-in thin-slicing Parratt formalism, which allows us to accurately account for the non-rectangular grating profile as well as variations in the depth profile of the polymer. The model solves the Schrödinger equation for the neutron wavefunction in each Parratt layer and sets the boundary conditions by imposing the continuity of the wavefunction and its derivative at the interfaces between adjacent layers.^{29,33} Combined with the “conservation of energy” condition for elastic

scattering events, this allows us to calculate the intensity of each reflected and transmitted beam and the detected polarization. Fits of the data to the dynamical theory (DT) model in the different integration schemes are shown in each of the panels in Fig. 3.

The DT fits were first performed on the SERGIS signals from the bare grating. The three fit parameters were found to be a grating period of $d = 808$ nm, a grating groove depth of $h = 130$ nm, and a grating blaze-angle of 10.25° , in good agreement with the manufacturer’s specifications and the AFM characterization of the grating ($d \sim 820$ nm). These values of the grating parameters were used in successive fits of the SERGIS data collected on the dPMMA coated grating and the subsequently thermally annealed sample. In the calculations, the scattering length density (SLD) of the dPMMA film was set to $7.09 \times 10^{-6} \text{ \AA}^{-2}$ and that of the Aluminum grating to $2.0 \times 10^{-6} \text{ \AA}^{-2}$. The calculations were performed using the same experimental incidence beam geometry with an incident angle of $\theta = 0.35^\circ$ relative to the surface of the grating. The angle ϕ of the incident beam relative to the grating lines was obtained from the best fit to the data and was found to be 0.1° , -0.2° , and 0.1° for the bare, “as cast,” and annealed samples, respectively. The beam divergence was treated as a Gaussian distribution with a standard deviation of 0.01° in θ and 0.27° in ϕ as calculated from slit settings. The DT fits to the data on the cast and annealed dPMMA films atop the grating reveal the degree to which the air–polymer interface conforms to the grating profile in both cases. We find that the cast film is draped over the grooves of the grating with a low degree of conformal correlation to the underlying grating structure. Although the best fits to the data were obtained for a slightly modulated free surface of the polymer film, an entirely flat polymer film profile is not expected in this case. In fact, a closer look at the intensity and polarization maps for the grating with the cast film [Figs. 2(b) and 2(e)] clearly shows an intense diffuse scattering signal compared to the

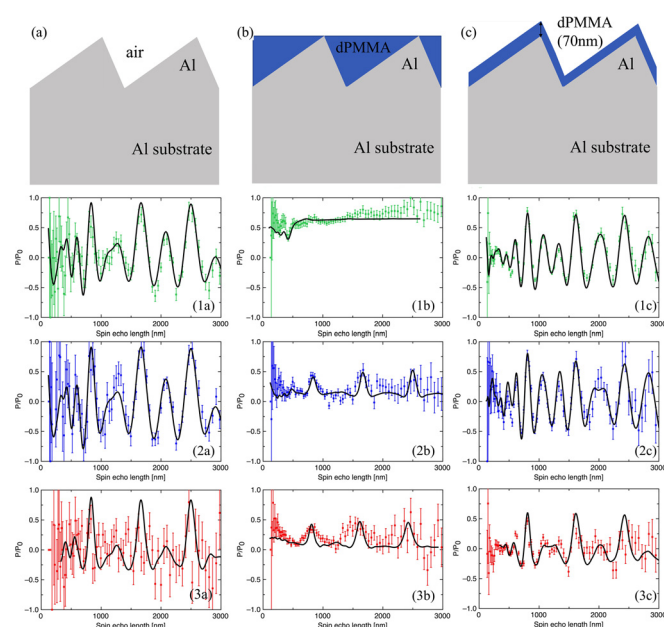


FIG. 3. Dynamical theory modeled data for the (a) bare grating (left column), (b) dPMMA buried grating (middle column), and subsequently thermally annealed buried grating (c) (right-hand column). Green is the integrated SERGIS signal across the entire detector maps 1a, 1b, and 1c, whereas blue is above (2a, 2b, and 2c) and red below (3a, 3b, and 3c) the specular ridge, respectively.

data maps for the bare grating [Figs. 2(a) and 2(d)]. This is a natural outcome of increased surface roughness of the polymer, as anticipated from the film floating deposition procedure (the details are given in the [supplementary material](#)). Indeed, the diffuse scattering effect is quite evident in the integrated polarization signal shown in Fig. 2(e). If the sample did not scatter diffusely, the observed plateau in the polarization signal should be close to one rather than ~ 0.6 (shown in panel 1b in Fig. 3). This loss of polarization also had to be accounted for in the data fitting by considering a scaling factor. Interestingly, despite the lack of features in the polarization signal integrated over the entire detector, the polarization signals obtained by excluding the specular ridge and integrating above and below specular show non-trivial modulations that systematically concur with the peak positions on the bare grating. The dynamical theory code accurately accounts for the off-specular polarization (integrated away from the specular ridge), which provides a theoretical corroboration of the polarization sensitivity of the SERGIS technique in detecting in-plane features from buried structures. This also indicates that the diffuse scattering from the film surface is mainly restricted to a region very close to the specular ridge, implying a large length-scale surface roughness as verified later using AFM [see Fig. S4(a)]. In contrast, the best DT fits on the annealed sample (1c, 2c, and 3c) reveal a scheme in which the polymer film faithfully complies with the underlying grating structure and forms a uniform coating, ~ 70 nm thick, which covers the aluminum grating surface as shown in the cartoon in Fig. 3(c).

The findings of the DT fitting were verified by AFM imaging of the samples in the as cast and annealed states (Fig. S4). AFM presents a clear corroboration of the surface structure of the coated gratings, but it does not provide information about the sub-surface structure

including the conformation of the polymer to the surface of the grating beneath, which is available through modeling of the SERGIS scattering data.

In summary, our results clearly show that SERGIS has strong sensitivity to periodic lateral structures that cannot otherwise be measured using conventional GISANS. Indeed, it is important to point out that GISANS can only detect in-plane structures over length scales of 1–500 nm (comparable to SANS), in which case the signal from a sample with larger periodicity would be obscured by the beam stop given the overall instrument length of current SANS instruments. For GISANS measurements on such samples to be possible, an unfeasibly long SANS instrument would be required. In contrast, SERGIS circumvents this issue by measuring the combined specular and off-specular scattering in the beam-stop region. Furthermore, masking off the purely specular scattering increases the sensitivity of the method, thereby confirming the theoretical prediction, as originally proposed by Felcher *et al.*²¹ Almost uniquely, SERGIS can probe buried periodic lateral structures with the data being accurately modeled using a powerful theoretical framework. In conclusion, we have made significant advances in the demonstration of the SERGIS technique as a truly unique and powerful probe of laterally structured materials and, importantly, even for the case of periodic nanostructures that are buried beneath the free surface of materials.

See the [supplementary material](#) for the descriptions of the grating sample preparation and annealing conditions, the OffSpec instrumental layout, and detector and polarizer setup. We also include a figure showing the SERGIS signal over-plotted to compare with and without excluding the specular region, annealed grating detector maps as a function of rocking angle, χ , specular reflectivity, and fit to determine the dPMMA layer thickness, as well as atomic force microscopy images before and after annealing the dPMMA layer on the grating. We also include the detector data for all three sample cases in reciprocal space plots. The Mathematica code used to model the SERGIS data using the Dynamical Theory (DT) is included.

AUTHOR'S CONTRIBUTIONS

R.M.D., R.A.L.J., A.D.F.D., and A.J.P. designed the initial experiment and were involved in writing the proposal for the beamtime. A.J.P., A.D.F.D., and R.M.D. carried out the neutron measurements. The SERGIS data analysis and discussion involved R.P., A.J.P., R.M.D., and R.A.; specifically, the SERGIS modeling was carried out by R.A. A.J.P. wrote the initial draft manuscript with input from all the authors.

The spin echo grazing incidence neutron experiments were supported by the STFC via the allocation of experimental time to use OffSpec (No. RB 1110285). A.J.P. was funded by the EPSRC Soft Nanotechnology Platform Grant (No. EP/E046215/1) and subsequently by a fellowship from the University of Sheffield. We thank Mr. Adam Hobson for assistance with the measurements on OffSpec. Dr. Nick Mullin helped with the AFM measurement of the annealed grating. A.J.P. is grateful to Dr. Steven Parnell for reading the draft manuscript and providing helpful comments.

REFERENCES

- ¹T. P. Russell, *Mater. Sci. Rep.* **5**, 171 (1990).
- ²G. Fragneto-Cusani, *J. Phys.* **13**, 4973 (2001).
- ³H. Zabel, *Physica B* **198**, 156 (1994).
- ⁴R. Pynn, S. M. Baker, G. Smith, and M. R. Fitzsimmons, *J. Neutron Res.* **7**, 139 (1999).
- ⁵F. Ott and S. Kozhevnikov, *IUCr, J. Appl. Cryst.* **44**, 359 (2011).
- ⁶R. M. Richardson, J. Webster, and A. Zarbakhsh, *J. Appl. Cryst.* **30**, 943 (1997).
- ⁷M. Sferrazza and S. Langridge, *Neutron News* **12**, 15 (2001).
- ⁸D. A. Styrkas, J. L. Keddie, J. R. Lu, T. J. Su, and P. A. Zhdan, *J. Appl. Phys.* **85**, 868 (1999).
- ⁹Y. Kamata, A. J. Parnell, P. Gutfreund, M. W. A. Skoda, A. J. C. Dennison, R. Barker, S. Mai, J. R. Howse, A. J. Ryan, N. Torikai, M. Kawaguchi, and R. A. L. Jones, *Macromolecules* **47**, 8682 (2014).
- ¹⁰G. H. Vineyard, *Phys. Rev. B* **26**, 4146 (1982).
- ¹¹S. Dietrich and H. Wagner, *Z. Phys. B* **56**, 207 (1984).
- ¹²S. Sinha, E. Sirota, S. Garoff, and H. Stanley, *Phys. Rev. B* **38**, 2297 (1988).
- ¹³J. P. de Silva, S. J. Martin, R. Cubitt, and M. Geoghegan, *Europhys. Lett.* **86**, 36005 (2009).
- ¹⁴M. S. Jablin, M. Zhernenkov, B. P. Toperverg, M. Dubey, H. L. Smith, A. Vidyasagar, R. Toomey, A. J. Hurd, and J. Majewski, *Phys. Rev. Lett.* **106**, 138101 (2011).
- ¹⁵R. Ashkar, V. O. de Haan, A. A. van Well, R. Dalgliesh, J. Plomp, M. R. Fitzsimmons, W. L. Schaich, and R. Pynn, *IUCr, J. Appl. Cryst.* **44**, 958 (2011).
- ¹⁶P. Müller-Buschbaum, *Polym. J.* **45**, 34 (2013).
- ¹⁷A. Hexemer and P. Müller-Buschbaum, *IUCr* **2**, 106 (2015).
- ¹⁸Z. Jiang, D. R. Lee, S. Narayanan, J. Wang, and S. K. Sinha, *Phys. Rev. B* **84**, 075440 (2011).
- ¹⁹H. Frielinghaus, M. Gvaramia, G. Mangiapia, S. Jaksch, M. Ganeva, A. Koutsoubas, S. Mattauch, M. Ohl, M. Monkenbusch, and O. Holderer, *Nucl. Inst. Methods Phys. Res., Sect. A* **871**, 72 (2017).
- ²⁰M. T. Rekveldt, *Physica B* **234–236**, 1135 (1997).
- ²¹G. P. Felcher, S. G. E. te Velthuis, J. Major, H. Dosch, C. Anderson, K. Habicht, and T. Keller, *Proc. SPIE* **4785**, 164 (2002).
- ²²J. Major, A. Vorobiev, A. Rühm, R. Maier, M. Major, M. Mezger, M. Nülle, H. Dosch, G. P. Felcher, P. Falus, T. Keller, and R. Pynn, *Rev. Sci. Instrum.* **80**, 123903 (2009).
- ²³A. Vorobiev, J. Major, H. Dosch, P. Müller-Buschbaum, P. Falus, G. P. Felcher, and S. G. E. te Velthuis, *J. Phys. Chem. B* **115**, 5754 (2011).
- ²⁴J. Plomp, V. O. de Haan, R. M. Dalgliesh, S. Langridge, and A. A. van Well, *Thin Solid Films* **515**, 5732 (2007).
- ²⁵R. M. Dalgliesh, S. Langridge, J. Plomp, V. O. de Haan, and A. A. van Well, *Physica B* **406**, 2346 (2011).
- ²⁶J. Plomp, “Spin-echo development for a time-of-flight neutron reflectometer,” Ph.D. thesis (Technische Universiteit Delft, Universal Press, Veenendaal, 2009).
- ²⁷A. J. Parnell, R. M. Dalgliesh, and R. A. L. Jones, *Appl. Phys. Lett.* **102**, 073111 (2013).
- ²⁸A. J. Parnell, A. Hobson, R. M. Dalgliesh, R. A. L. Jones, and A. D. F. Dunbar, *J. Visualized Exp.* **83**, e51129 (2014).
- ²⁹R. Ashkar, W. L. Schaich, V. O. de Haan, A. A. van Well, R. Dalgliesh, J. Plomp, and R. Pynn, *J. Appl. Phys.* **110**, 102201 (2011).
- ³⁰R. Gähler, R. Golub, K. Habicht, T. Keller, and J. Felber, *Physica B* **229**(1), 1 (1996).
- ³¹R. Ashkar, R. Pynn, R. Dalgliesh, N. V. Lavrik, and I. I. Kravchenko, *J. Appl. Cryst.* **47**, 1367–1373 (2014).
- ³²R. Ashkar, “Dynamical theory applications to neutron scattering from periodic nanostructures,” Ph.D. thesis (Indiana University, 2012).
- ³³R. Ashkar, P. Stonaha, A. L. Washington, V. R. Shah, M. R. Fitzsimmons, B. Maranville, C. F. Majkrzak, W. T. Lee, W. L. Schaich, and R. Pynn, *J. Appl. Cryst.* **43**, 455 (2010).